

The spectral function of composites: the inverse problem

A R Day^{†§} and M F Thorpe[‡]

[†] Physics Department, Marquette University, Milwaukee, WI 53233, USA

[‡] Department of Physics & Astronomy and Center for Fundamental Materials Research, Michigan State University, East Lansing, MI 48824, USA

Received 16 December 1998

Abstract. The dielectric function of a composite depends on the geometry of the composite and the dielectric functions of the constituent materials. In the Bergman–Milton spectral representation for a two-component composite, all of the relevant geometric information can be captured in a spectral function which is independent of the material properties. Extracting the spectral function from experimental values of the dielectric function would be a compact way of presenting a large body of data and highlight the role of geometry in determining the electrical properties of the composite. We show that known constraints on the spectral function make it possible to solve the inverse problem of determining the spectral function directly from experimental measurements of the reflectance if one of the components has a resonance and data are taken in the reststrahlen band, where the real part of the dielectric function of the optically active material is negative. We demonstrate the method using numerical simulations of the reflectance of a model system with physically reasonable values for the dielectric functions of the two components. Our results show that the spectral function determined by this method is stable against the introduction of noise and agrees with that previously calculated directly for the same model geometry. We suggest that this technique will be useful when used with real experimental data.

1. Introduction

The problem of calculating the dielectric constant of a composite material is an old one, dating back to Maxwell [1], and was already a mature subject by the 1970s [2, 3]. It has continued to be a subject of active research, driven by the increasing importance of composite materials. A significant theoretical advance was the spectral representation for the dielectric function of a two-phase composite, independently developed by Bergman [4] and Milton [5]. This mathematically elegant representation has the appealing property of separating the influence of the geometry of the composite from the influence of dielectric properties of the constituent components. The spectral function of a composite would be a compact way of representing experimental data taken over a range of frequencies and would highlight the role of geometry in determining the effective properties. It could also provide a link between data taken at different temperatures for the same composite material or even completely different properties like the dielectric function and the magnetic permeability, which will depend on the composite geometry in the same way. Despite this, applications to the analysis of real experimental data have been mainly limited to calculating bounds on the dielectric function of the composite, although there have been two attempts [6, 7] to fit the dielectric response of brine-saturated rock using an analytic form for the spectral function.

§ Author to whom any correspondence should be addressed. E-mail address: dayroy@marquette.edu.

In this paper we develop a method for extracting the spectral function directly from experimental measurements, which can be regarded as an inverse problem [8, 9]. In this initial paper, we will use simulated data but we plan in subsequent publications to apply the technique to actual experimental data. By doing numerical simulations of a two-dimensional (2d) square net with random site substitution, we will demonstrate that it is possible to solve the inverse problem of determining the spectral function from the dielectric functions of the pure materials and dielectric properties of the composite. Our results are in good agreement with the spectral function obtained previously by direct methods [10]. A key result of this work is the stability of the spectral function against the introduction of noise, both in the simulated dielectric properties of the composite and in the assumed values for the dielectric functions of the pure materials. Finally, we will discuss possible experiments that would provide a test of this approach using real data.

2. The spectral function

Consider a two-component composite and label the components A and B, with dielectric constants ε_A , and ε_B , respectively. The dielectric constants are, in general, complex functions of the frequency ω . The composite has a dielectric constant ε which depends on ε_A , ε_B , and the geometry of the composite. If we consider A to be the host, and B to be the inclusion, we define the complex variable

$$s_A = \frac{1}{1 - \varepsilon_B/\varepsilon_A} \quad (1)$$

and define the scaled dielectric function of the composite to be $m_A = \varepsilon/\varepsilon_A$. The spectral function $h_A(x)$ is defined via the integral [4, 5, 10–12]

$$m_A(s_A) = 1 - \int_0^1 \frac{h_A(x) dx}{s_A - x}. \quad (2)$$

The spectral function $h_A(x)$ is a positive real function of a real variable x , and is only non-zero in the interval $0 \leq x < 1$. It can be interpreted as the density of poles of the dielectric function of the composite [10, 11], and contains all of the geometrical information required to determine m . In the thermodynamic limit, the line of singularities on the real interval $x \in [0, 1]$ becomes a cut on the real axis in the complex s -plane and $h_A(x)$ is the discontinuity of m_A across the cut [6].

Equivalently we could consider B to be the host and A the inclusion. In this case we would have

$$s_B = \frac{1}{1 - \varepsilon_A/\varepsilon_B} \quad (3)$$

and define the scaled dielectric function of the composite to be $m_B = \varepsilon/\varepsilon_B$. The spectral function $h_B(x)$ is defined via the integral

$$m_B(s_B) = 1 - \int_0^1 \frac{h_B(x) dx}{s_B - x}. \quad (4)$$

We show in appendix A that the spectral function $h_A(x)$ contains a delta function at $x = 0$ with weight

$$\sigma_B = m_B(1) = 1 - \int_0^1 \frac{h_B(x) dx}{1 - x} \quad (5)$$

which is the dielectric function of the composite if $\varepsilon_A = 0$, and $\varepsilon_B = 1$. We use the notation $\sigma_B = m_B(1)$ to emphasize that σ_B is also the conductivity of the composite in the percolation

problem [13] when the A phase is a void, and the B phase has unit conductivity [7]. The delta function in h_A (when A is the host) only has non-zero weight when the B phase (the inclusion) percolates. Similarly, $h_B(x)$ contains a delta function at $x = 0$ with weight

$$\sigma_A = m_A(1) = 1 - \int_0^1 \frac{h_A(x) dx}{1-x} \tag{6}$$

which is the dielectric function of the composite if $\epsilon_B = 0$, and $\epsilon_A = 1$. The delta function in h_B (when B is the host) only has non-zero weight when the A phase (the inclusion) percolates. Note that while m_A, m_B , and s are in general complex, σ_A, σ_B , and x are always real.

The definition of the spectral function has a simple dependence on which material, A or B, is arbitrarily chosen as the host, because from (1) and (3)

$$s_A + s_B = 1 \tag{7}$$

and we show in appendix A that

$$xh_A(x) = (1-x)h_B(1-x). \tag{8}$$

This suggests the definition of a new function

$$g(x) = xh_A(x) = (1-x)h_B(1-x) \tag{9}$$

which we will call the *reduced spectral function*. The reduced spectral function, $g(x)$, has the advantage of separating the delta function at the origin from the rest of the spectral function [14]. The function $g(x)$ is finite everywhere and goes to zero at both $x = 0$ and $x = 1$, as we will show later. The spectral functions, h_A and h_B , are then written in terms of g as

$$h_A(x) = \frac{g(x)}{x} + \sigma_B \delta(x) \tag{10}$$

and

$$h_B(x) = \frac{g(1-x)}{x} + \sigma_A \delta(x). \tag{11}$$

The properties of the spectral function have been extensively studied and a number of constraints are known [4, 5, 10, 11], which we summarize. All of the moments of h exist and in particular the zeroth moment satisfies

$$\begin{aligned} \mu_0^A &= \int_0^1 h_A(x) dx = p_B \\ \mu_0^B &= \int_0^1 h_B(x) dx = p_A \end{aligned} \tag{12}$$

where p_A is the volume fraction of component A and $p_B = 1 - p_A$ is the volume fraction of component B. Clearly

$$\mu_0^A + \mu_0^B = p_A + p_B = 1. \tag{13}$$

The first moment is the same for both spectral functions,

$$\mu_1 = \int_0^1 xh_A(x) dx = \int_0^1 xh_B(x) dx \tag{14}$$

and for an isotropic material μ_1 always has the form

$$\mu_1 = p_w p_A p_B \tag{15}$$

where the parameter p_w is determined from the weak-scattering limit when the difference between the dielectric constants of the two materials, A and B, is small [15]. For a macroscopically isotropic continuum composite in d dimensions, with *any* inclusion geometry,

$p_w = 1/d$, as shown by Landau and Lifshitz [16]. For lattice problems there is a connection between the weak-scattering limit and dilute limit [10, 17] and $p_w = p_I$, where p_I is the initial slope of the conductivity in the percolation problem. The initial slope can be calculated for most lattice problems [18]. For example, a hypercubic lattice in d dimensions with random bond substitution has $p_w = p_I = 1/d$, and the 2d square net with random site substitution has $p_w = p_I = 1 - 1/\pi$, which we use later in this paper. We therefore treat p_w as a known quantity.

The spectral function, $h(x)$, may diverge in the limit $x \rightarrow 0$ but because $h_A(x)$ is normalizable, any singularity at $x = 0$ must be integrable and thus $\lim_{x \rightarrow 0} x h_A(x) = 0$. From equation (8) this implies $\lim_{x \rightarrow 1} h_B(x) = 0$. Similarly, $\lim_{x \rightarrow 0} x h_B(x) = 0$ implies $\lim_{x \rightarrow 1} h_A(x) = 0$.

From the properties of the spectral function, we deduce that the reduced spectral function $g(x)$ is also real and positive and that all of the moments of g exist. From the constraints on the zeroth moments of $h(x)$ we obtain

$$\begin{aligned} \sigma_B + \int_0^1 \frac{g(x) dx}{x} &= p_B \\ \sigma_A + \int_0^1 \frac{g(1-x) dx}{x} &= p_A \end{aligned} \quad (16)$$

and by adding these two equations we have

$$\sigma_B + \sigma_A + \int_0^1 \frac{g(x) dx}{x(1-x)} = 1. \quad (17)$$

The first moment of h can be rewritten as

$$\mu_1 = \int_0^1 g(x) dx = p_w \left(\sigma_B + \int_0^1 \frac{g(x) dx}{x} \right) \left(\sigma_A + \int_0^1 \frac{g(1-x) dx}{x} \right). \quad (18)$$

Finally, the limits on $h(x)$ at $x = 0$ and $x = 1$ imply

$$g(0) = g(1) = 0 \quad (19)$$

which is also required by equation (17).

3. Determining the spectral function from experimental data

3.1. General considerations

If $\varepsilon_A(\omega)$, $\varepsilon_B(\omega)$, and $\varepsilon(\omega)$ are known, the problem of determining the spectral function is equivalent to solving the inverse problem of extracting $h(x)$ from

$$m(s) = 1 - \int_0^1 \frac{h(x) dx}{s-x}. \quad (20)$$

where s is a function of ω . This is an example of an inhomogeneous Fredholm equation [8] of the first kind and, as is frequently the case [9], the kernel $K(s, x) = 1/(s-x)$ is sufficiently ill-conditioned that experimental noise in m will result in a meaningless, wildly oscillating solution for h . The standard method of dealing with this problem is to include *a priori* knowledge about the solution into the kernel, a process known as regularization [8, 9]. The simplest form of regularization usually involves some assumption about the smoothness of the solution, but any *a priori* knowledge can be included. As we will show below, the known properties of the spectral function discussed in section 2 provide sufficient *a priori* knowledge to regularize the kernel.

In addition to the problem of regularization, there is the problem of loss of information when we take data at a discrete set of data points. The integral transform, equation (20), is a smoothing or broadening process and, even in principle, it is only possible to do the complete unfolding for a continuum of data. To minimize this loss of information we would like the kernel, or broadening function, to be as sharp as possible. This is achieved when the data are taken for values of s that are close to the cut $x \in [0, 1]$. In previous work [10] we determined the spectral function for random networks by doing numerical simulations of m on a track just above the cut. The imaginary part of the resulting m was the spectral function, convoluted with a narrow Lorentzian function.

In an actual experiment, the s -values are determined by the dielectric functions of the two components. We obtain the desired s -track, that passes near to the cut, if there are data over a frequency range where $\text{Re}(\varepsilon_A/\varepsilon_B) < 0$ which can be achieved if at least one of the materials has at least one resonance. A convenient case is that when there is a resonance in one material, while the other material is essentially inert. For example, suppose component B has a constant real dielectric function $\varepsilon_B(\omega) = \varepsilon_B$ and component A has a resonance at a frequency ω_{TO} . For frequencies between the transverse optic frequency, ω_{TO} , and the longitudinal optic frequency, ω_{LO} , the real part of ε_A is negative and s follows a track just above or just below the cut $x \in [0, 1]$. Thus, the data in this reststrahlen band [19] will be the best data for the inverse problem of extracting h from m . The distance from the track to the cut (i.e. the imaginary part of s) is proportional to the width of the resonance and consequently a sharp resonance line is best for extracting the spectral function. As with the numerical simulations [10], if the linewidth is very narrow the spectral function is simply proportional to the imaginary part of m [20]. Previous attempts at obtaining the spectral function from the dielectric function of brine-saturated rock [6, 7] have had limited success because the data were taken at values of s away from the branch cut, and thus could not resolve the structure in the spectral function.

For most materials, direct measurement of the dielectric function at the appropriate frequencies (between ω_{TO} and ω_{LO}) is not possible. The experimentally accessible quantity is the reflectance at normal incidence, $R(\omega)$, which is related to the dielectric function via

$$R = \left| \frac{\sqrt{\varepsilon} - 1}{\sqrt{\varepsilon} + 1} \right|^2. \quad (21)$$

The complex dielectric constant can be obtained from the complex reflectivity, $r = \rho e^{i\theta}$, where $\rho = \sqrt{R}$. If $R(\omega)$ is measured over a wide frequency range the phase shift $\theta(\omega)$ can be determined by extrapolating the data to low and high frequencies and performing a Kramers–Kronig analysis. Although this is a standard procedure [21] it does introduce additional errors into ε so we bypass the Kramers–Kronig analysis and extract the spectral function directly from reflectance data. This results in a very non-linear inversion problem but this complication is more than compensated for by the fact that we only use measured data, and no extrapolations are needed. It has the added advantage that the constraints imposed on the spectral function guarantee that the resulting dielectric function of the composite satisfies the Kramers–Kronig relations [22], and the Bergman–Milton bounds [4, 5].

3.2. The numerical algorithm

We develop an algorithm to determine the spectral function by doing a non-linear least-squares fit to reflectance data with additional constraints imposed to ensure that the spectral function has all of the properties listed in section 2. We minimize the *chi-squared* function

$$\chi^2 = \chi_{\text{constraint}}^2 + \chi_R^2 \quad (22)$$

where the function $\chi_{\text{constraint}}^2$ imposes the constraints of section 2 and the function χ_R^2 is defined as

$$\chi_R^2 = \sum_k \left(\frac{R_k - R(\omega_k, \varepsilon_A, \varepsilon_B, g, \sigma_A, \sigma_B)}{\sigma_k} \right)^2. \quad (23)$$

The R_k and σ_k are experimental values for the reflectance and their standard deviations, taken at a set of frequencies ω_k . The function $R(\omega_k, \varepsilon_A, \varepsilon_B, g, \sigma_A, \sigma_B)$ determines the reflectance at the points $s_k = s(\omega_k)$. It depends on the *known* dielectric functions of the pure materials, $\varepsilon_A(\omega_k)$ and $\varepsilon_B(\omega_k)$, and the *unknown* spectral function, expressed as the reduced spectral function, $g(x)$, and the weights of the delta functions, σ_A and σ_B . The unknowns are adjusted to obtain the best fit to the data, subject to the constraints. The algorithm is highly non-linear because we must first calculate $\varepsilon(g, \sigma_A, \sigma_B, \varepsilon_A, \varepsilon_B)$ and then calculate $R(\varepsilon)$ using equation (21). The dielectric function of the composite is calculated in a completely symmetric way, that makes no distinction between host and inclusion, via

$$\varepsilon(\omega) = \frac{1}{2} \varepsilon_A \left(1 - \frac{\sigma_B}{s_A} - \int_0^1 \frac{g(x) dx}{x(s_A - x)} \right) + \frac{1}{2} \varepsilon_B \left(1 - \frac{\sigma_A}{s_B} + \int_0^1 \frac{g(1-x) dx}{x(s_B - x)} \right). \quad (24)$$

The function $\chi_{\text{constraint}}^2$ is defined as

$$\begin{aligned} \chi_{\text{constraint}}^2 = & \lambda_1 \left| \sigma_A + \sigma_B + \int_0^1 \frac{g(x) dx}{x(1-x)} - 1 \right|^2 \\ & + \lambda_2 \left| p_w \left(\sigma_B + \int_0^1 \frac{g(x) dx}{x} \right) \left(\sigma_A + \int_0^1 \frac{g(1-x) dx}{x} \right) - \int_0^1 g(x) dx \right|^2 \\ & + \lambda_{\text{smooth}} |\nabla g(x)|^2 \end{aligned} \quad (25)$$

where the first two terms impose the *a priori* knowledge of $g(x)$ from equations (17) and (18) and the third term is a smoothing term that can be included as necessary. The λ_i are Lagrange multipliers which can be adjusted for stability, as will be discussed in section 4.2. Note that these constraints do not involve any experimental information about the composite geometry, not even the volume fractions which will be obtained from the fit to the data. We assume that p_w is known which will be the case for most composites of interest, as discussed in section 2. For example, $p_w = 1/3$ for all macroscopically isotropic continuum composites.

The minimization is implemented using a Levenberg–Marquardt algorithm [23] written so as to forbid negative values for σ_A , σ_B , and $g(x)$. The weights of the delta functions, σ_A and σ_B , are discrete variables and we use a histogram representation for $g(x)$. The gradient term in equation (25) is represented as a finite-difference operator and within the histogram representation of the reduced spectral function g , the integrations are done exactly. Because the minimization process is non-linear, we average over the results obtained from several different initial guesses for $g(x)$.

We conclude this section with a few comments on experimental considerations. It is worth making a considerable effort to determine ε_A and ε_B as accurately as possible because errors in ε_A and ε_B propagate through the solution. This suggests that for the pure system, reflection data should be taken over the widest frequency range possible before performing the Kramers–Kronig analysis to obtain the real and imaginary parts of the dielectric function. Or, if possible, ellipsometry should be used to determine the real and imaginary parts directly [24]. It is less important to measure the reflectance of the composite over an extended frequency range because no Kramers–Kronig analysis is required. Away from the reststrahlen band the dielectric functions ε_A and ε_B are both real, and are often similar in magnitude. Under these conditions the dielectric function ε is essentially determined by the Hashin–Shtrikman bounds [25], which

are very tight when ε_A and ε_B have similar magnitudes. We also note that although the principal goal in this work is to develop a method for determining the spectral function, this approach also gives a useful method of extracting the dielectric function from the reflectance for the special case of a two-component composite, where the dielectric functions of the pure materials are known. By including the additional input of the dielectric functions of the pure materials, ε_A and ε_B , the method is superior to one relying only on the reflectance of the composite. By construction, the dielectric function of the composite will satisfy the Kramers–Kronig relationship and all bounds that depend on only the isotropy of the composite and the volume fractions. An inability to obtain a good fit to the data would indicate problems in the reflectance data, the dielectric functions of the pure materials, the assumption that the data are for a two-component material, or some combination of these three.

4. Numerical test of the method

4.1. The model

We have tested the algorithm using data generated by numerical simulations on a 2d square network with random site substitution, as shown in figure 1. Sites are randomly chosen to be type A with probability p_A and type B with probability $p_B = 1 - p_A$. Bonds connecting two A sites have a dielectric function ε_A , bonds connecting two B sites have dielectric function ε_B , and bonds connecting an A site to a B site have a dielectric function $2\varepsilon_A\varepsilon_B/(\varepsilon_A + \varepsilon_B)$, so the model is completely symmetric under an $A \leftrightarrow B$ and $p_A \leftrightarrow p_B$ interchange. For material A we assign a dielectric function $\varepsilon_A(\omega)$ that exhibits a single resonance line and assign a constant value for ε_B . This results in $s(\omega)$ following a track in the complex s -plane that passes near the cut $x \in [0, 1]$. At each probability we calculate the dielectric function of the composite $\varepsilon(\omega)$ for a range of frequencies that sweep through the resonance line of material A. From the dielectric function we determine the reflectance

$$R(\omega) = |(\sqrt{\varepsilon} - 1)/(\sqrt{\varepsilon} + 1)|^2.$$

We then regard $R(\omega)$ as the *experimental* data and proceed with the inverse problem of determining the spectral function from these data. The direct simulations were done on a 128-

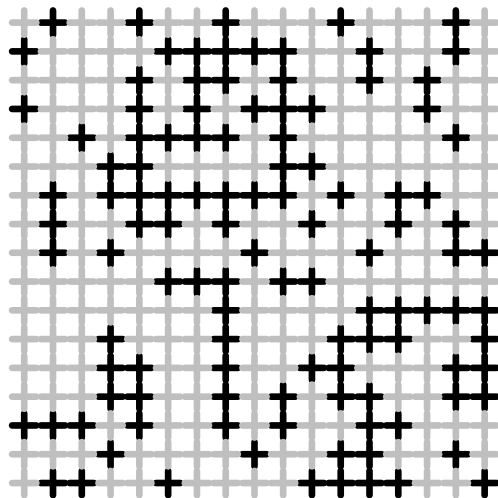


Figure 1. A 2d square net with random site substitution.

by-128 square lattice at 500 frequencies and averaged over 64 realizations at each probability. The dielectric function of the composite is calculated using a $Y-\Delta$ transformation [26], where we consider each bond to have an appropriate complex impedance, and we calculate the equivalent impedance of the network.

Because actual experimental data will always have some random noise, and perhaps systematic errors, our test is only valid if we introduce noise into the data. We note that there are two sources of error. There are errors in the assumed values for the dielectric functions of the pure materials, ε_A and ε_B , which lead to errors in $s(\omega)$, and there are errors in the composite property, $R(\omega)$. Errors in ε_A and ε_B are the most damaging because they propagate through every step of the calculation and, as discussed in the previous section, they are the most difficult to reduce because we need both the real and imaginary parts of the dielectric functions of the pure material.

We introduce errors into our simulated data in two ways. We calculate $R(\omega)$ exactly using a model where the A material has a dielectric function $\varepsilon_{\text{true}}(\omega)$ which exhibits a single resonance line, and the B material has a frequency-independent dielectric constant $\varepsilon_B = 10$. The reflectance data already include some noise, because we only average over 64 random samples at each probability, but we add additional noise with a maximum amplitude of 0.02, as discussed in appendix B. We do the analysis using a noisy value for ε_A , as discussed below.

We introduce noise into ε_A in the following way. To material A we assign a dielectric function consisting of two closely spaced Lorentz oscillators which results in a dielectric function with the appearance of a single resonance line. The dielectric function can be written as

$$\varepsilon_{\text{true}}(\omega) = \varepsilon_{\infty} \left(1 + \frac{\omega_{P,1}^2}{\omega_{TO,1}^2 - \omega^2 - i\gamma_1\omega} + \frac{\omega_{P,2}^2}{\omega_{TO,2}^2 - \omega^2 - i\gamma_2\omega} \right). \quad (26)$$

We choose $\varepsilon_{\infty} = 5.0$ and, for the first oscillator, $\omega_{P,1} = 173.2 \text{ cm}^{-1}$, $\omega_{TO,1} = 299 \text{ cm}^{-1}$, and $\gamma_1 = 10.2 \text{ cm}^{-1}$. For the second oscillator we choose $\omega_{P,2} = 223.6 \text{ cm}^{-1}$, $\omega_{TO,2} = 301 \text{ cm}^{-1}$, and $\gamma_2 = 9.8 \text{ cm}^{-1}$. We then calculate $R(\omega)$ from $\varepsilon_{\text{true}}(\omega)$ and add some noise to the reflectance. Finally, we fit this noisy reflectance curve with a *single* Lorentz oscillator of the form

$$\varepsilon_A(\omega) = \varepsilon_{\infty} \left(1 + \frac{\omega_P^2}{\omega_{TO}^2 - \omega^2 - i\gamma\omega} \right) \quad (27)$$

which is used in the analysis. The fitted $\varepsilon_A(\omega)$ has $\varepsilon_{\infty} = 5.217$, $\omega_P = 282.4 \text{ cm}^{-1}$, $\omega_{TO} = 300.6 \text{ cm}^{-1}$, $\gamma = 9.860 \text{ cm}^{-1}$, and $\omega_{LO} = \sqrt{\omega_P^2 + \omega_{TO}^2} = 412.5 \text{ cm}^{-1}$. This results in an error of about 4% in ε_A at high and low frequencies, but with a much smaller percentage error near the resonance peak. We consider this error in $\varepsilon_A(\omega)$, and the resulting error in $s(\omega)$, to be systematic error.

Figure 2 is a plot of the reflectance of the pure A system. We show the true reflectance as calculated from $\varepsilon_{\text{true}}(\omega)$, the reflectance with noise added, and the fitted reflectance that gives $\varepsilon_A(\omega)$. These curves indicate that the errors introduced have magnitudes that are probably representative of real experimental errors.

Figure 3 is a plot in the complex s -plane of both $s_{\text{true}}(\omega)$ (calculated from $\varepsilon_{\text{true}}(\omega)$ and ε_B) and $s(\omega)$ (calculated from the fitted $\varepsilon_A(\omega)$, and ε_B) which is used in the analysis. The two curves are similar in the frequency range $300 \text{ cm}^{-1} < \omega < 400 \text{ cm}^{-1}$ where they are closest to the cut, except that there is a kink in the $s_{\text{true}}(\omega)$ curve (caused by the double oscillator) near 300 cm^{-1} , and the two curves are slightly offset (by about $x = 0.01$ near $\omega = 350 \text{ cm}^{-1}$). The $s(\omega)$ track is completely determined by the properties of the pure materials and is the same for each set of data (i.e. each probability p). We show both $s_A(\omega)$ (in the lower half-plane) and $s_B(\omega)$ (in the upper half-plane) and indicate the approximate frequency at various points on

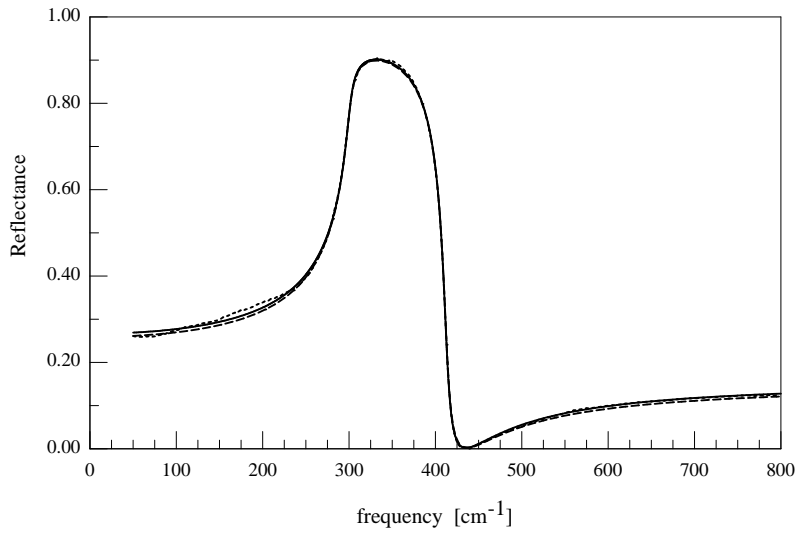


Figure 2. The reflectance of the pure A system as a function of the frequency. The broken curve (---) is $R_{\text{true}}(\omega)$, as calculated from ϵ_{true} (equation (26)). The dashed curve (- - -) is $R_{\text{true}}(\omega)$ with noise added. The solid curve (—) is the fitted $R(\omega)$, which gives $\epsilon_A(\omega)$ (equation (27)), as discussed in section 4.1.

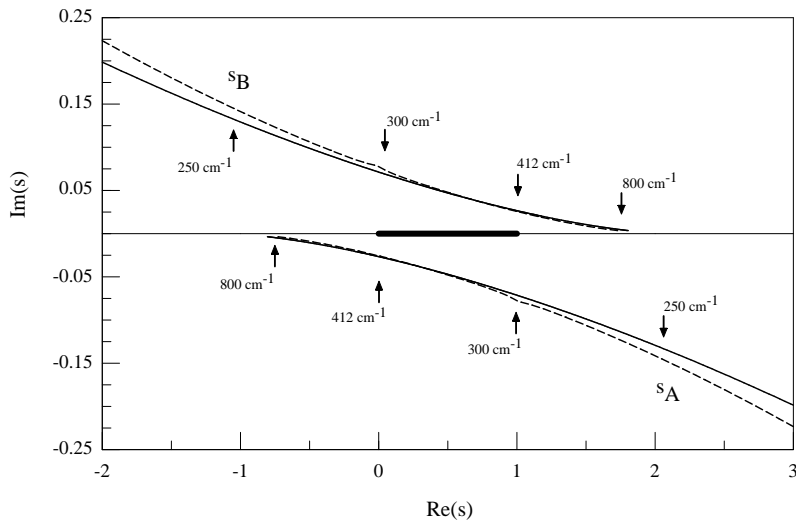


Figure 3. A plot of the complex variable $s(\omega)$ for the model system. The broken curve (---) is the curve $s_{\text{true}}(\omega)$, calculated from the true dielectric constants $\epsilon_{\text{true}}(\omega)$ and ϵ_B . The solid curve (—) is the value of $s(\omega)$ obtained using the noisy $\epsilon_A(\omega)$, as discussed in section 4.1. The arrows indicate the approximate frequencies at various points on the track and the thick line indicates the cut $x \in [0, 1]$. The curves in the upper half-plane are s_B , where B is taken as the host; the curves in the lower half-plane are s_A , where A is taken as the host.

the curves. Because $s_A + s_B = 1$ the two tracks are related by a reflection about the x - (real) axis, followed by a reflection about the line $x = 0.5$. The thick line on the real axis indicates the cut where the spectral function $h(x)$ is non-zero.

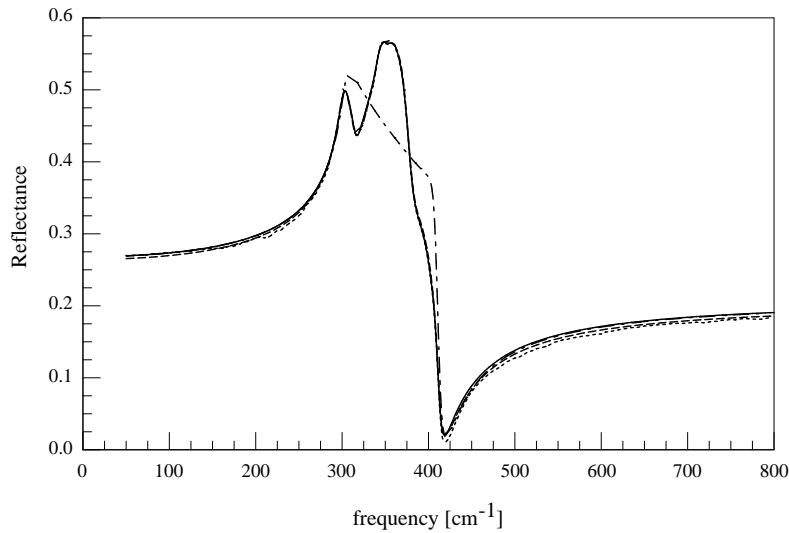


Figure 4. The reflectance, $R(\omega)$, of a 2d square net with random site disorder and the concentration $p_A = 0.50$. The broken curve (---) is the true reflectance, $R_{\text{true}}(\omega)$, as calculated by the simulations. The dashed curve (- - -) is $R_{\text{true}}(\omega)$ with noise added. The solid curve (—) is the fitted $R(\omega)$, which is used to determine the spectral function. The dash-dot curve (- · -) is the effective-medium-theory curve.

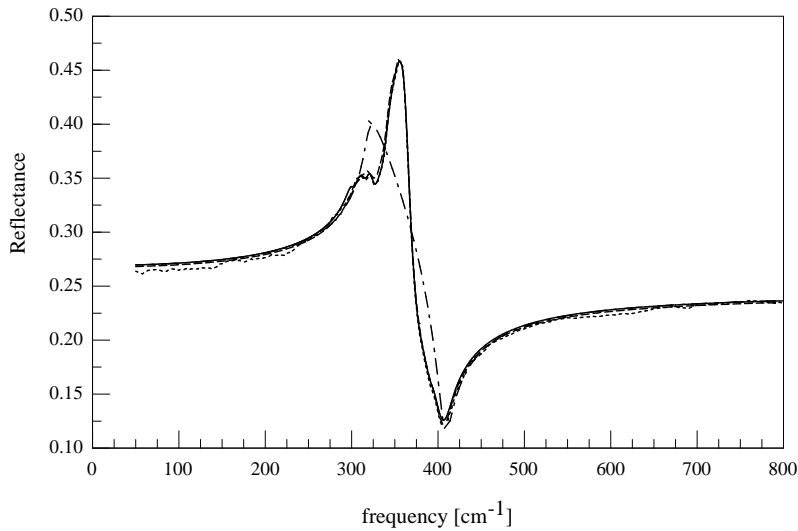


Figure 5. The reflectance, $R(\omega)$, of a 2d square net with random site disorder and the concentration $p_A = 0.20$. The broken curve (---) is the true reflectance, $R_{\text{true}}(\omega)$, as calculated by the simulations. The dashed curve (- - -) is $R_{\text{true}}(\omega)$ with noise added. The solid curve (—) is the fitted $R(\omega)$, which is used to determine the spectral function. The dash-dot curve (- · -) is the effective-medium-theory curve.

4.2. Results

We compute data for the reflectance of our model composite at eleven different concentrations from $p_A = 0.05$ to $p_A = 0.95$. At each concentration we add additional noise as discussed

in appendix B. From the noisy reflectance data we extract the spectral function using the algorithm described in section 3.2, representing the reduced spectral function, $g(x)$, by a 100-bin histogram. At each concentration we average over the results obtained from ten different initial guesses for the spectral function, where the initial guess is a set of random values scaled such that the first moment is approximately correct. Because most published reflectance data do not give values for the experimental standard deviations, σ_k , we set all $\sigma_k = 1$. The constraints have weights $\lambda_1 = \lambda_2 = \lambda = 1$ and $\lambda_{\text{smooth}} = 0.1$. The fit is largely insensitive to the actual value for λ , but the relative weighting of the smoothing term is important, as is discussed below.

Figures 4, 5, 6, and 7 show examples of the reflectance, $R(\omega)$, and the reduced spectral function, $g(x)$, for $p_A = 0.50$ and $p_A = 0.20$, which are representative of the complete data set. In the reflectance figures (figures 4 and 5) we plot the true reflectance as calculated in the simulations, the reflectance with noise added, the reflectance fitted to the noisy data, and the effective-medium-theory reflectance which is calculated using the noisy $\varepsilon_A(\omega)$ and ε_B . Notice that the noise is appreciable, and that the fit is generally good, especially in the restrahlen band, $\omega_{TO} < \omega < \omega_{LO}$. The effective-medium reflectance is a very poor fit in this region, but it is a better fit well away from the resonance line. In contrast, away from the resonance line the fitted reflectance and the effective-medium reflectance are essentially the same. This is because away from the resonance ε_A and ε_B are both real and thus the dielectric constant ε (and hence the reflectance R) must satisfy the Hashin–Shtrikman bounds [25]. Because ε_A and ε_B only differ by a factor of two away from the resonance, these bounds are very tight and, of course, contain the effective-medium-theory result. By construction, the fitted reflectance curve must satisfy the Hashin–Shtrikman bounds so it must be close to the effective-medium curve. It will not necessarily coincide with the true reflectance, because the bounds are calculated using the noisy $\varepsilon_A(\omega)$ and ε_B .

The reduced spectral function, $g(x)$, extracted from the reflectance data with noise added and using the using the noisy $\varepsilon_A(\omega)$ and ε_B , is plotted in figures 6 and 7. These figures

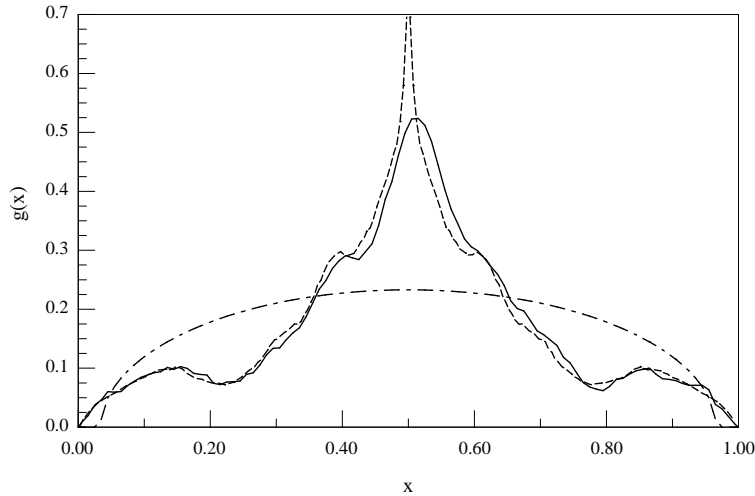


Figure 6. The reduced spectral function $g(x)$ for the 2d square net with random site disorder at $p_A = 0.50$. The broken curve (---) is $g_0(x)$, as calculated in reference [10]. The solid curve (—) is the $g(x)$ obtained from the reflectance data of figure 4. The dash-dot curve (— · —) is the effective-medium-theory curve.

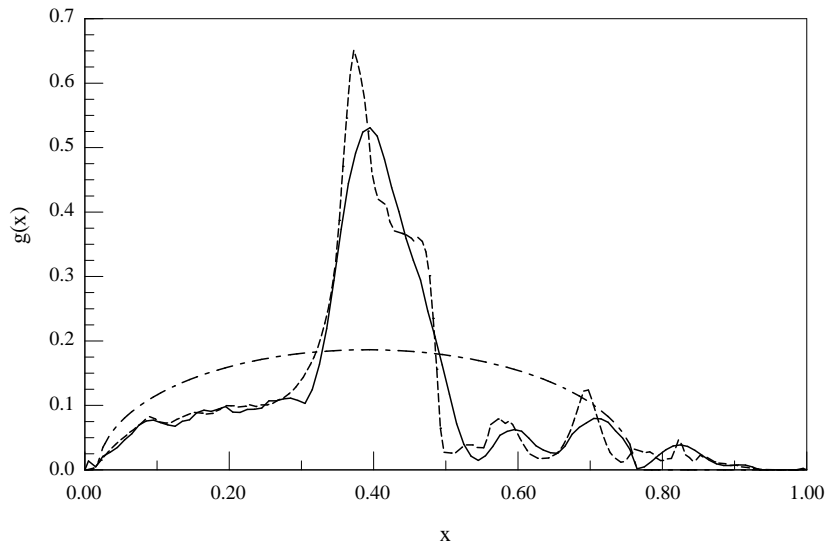


Figure 7. The reduced spectral function $g(x)$ for the 2d square net with random site disorder at $p_A = 0.20$. The broken curve (---) is $g_0(x)$, as calculated in reference [10]. The solid curve (—) is the $g(x)$ obtained from the reflectance data of figure 5. The dash-dot curve (- · -) is the effective-medium-theory curve.

also contain the curve $g_0(x)$, which is the reduced spectral function as calculated directly in reference [10], and the effective medium $g(x)$. It is clear that the fitted $g(x)$ reproduces the major features of $g_0(x)$ with some structure smoothed out, and some additional noise. The major peak of the reduced spectral function g is slightly shifted from its true position which is a systematic error related to the offset in the $s(\omega)$ curve, discussed in section 4.1. For a symmetric lattice model the reduced spectral function should have the symmetry $g(x, p) = g(1-x, 1-p)$. As can be seen from the $p_A = 0.5$ curve shown in figure 6 (which should be symmetric about $x = 0.5$) this symmetry is approximately satisfied, with deviations caused by the noise in the simulated experimental data. As would be expected, the errors in the fitted $g(x)$ are reduced if the noise in the model is reduced, but it is apparent that we can extract a meaningful $g(x)$ from quite noisy data. If we increase the noise the quality of the fitted $g(x)$ is reduced but even with four times as much noise most of the structure remains. Finally, we note that the fitting procedure produces a much better reduced spectral function than does effective-medium theory.

The delta functions are removed from the reduced spectral function but their weights are also obtained from the fitting procedure. In figure 8 we plot the weights σ_A and σ_B for the eleven values of p_A . The solid curves are $\sigma_A(p)$ and $\sigma_B(p)$ from the percolation problem [27] which can be calculated directly. The curve for $\sigma_A(p)$ is zero, when p_A is less than the percolation threshold $p_c = 0.593$ [13]. At the percolation threshold, σ_A starts increasing from zero to reach unity when $p_A = 1$. For a symmetric lattice model, the curves for σ_A and σ_B are mirror images about the line $p = 1/2$, and $\sigma_B(p)$ goes from 1 when $p_A = 0$ to zero at $p_A = 1 - p_c = 0.407$. Separating the delta function at the origin from weight in the spectral function near $x = 0$ is a demanding test of the analysis but, as seen in figure 8, the results are rather good.

As an additional check on the accuracy of the fitted spectral function we give the values of the zeroth and first moments, together with the theoretical values for the moments, in table 1.

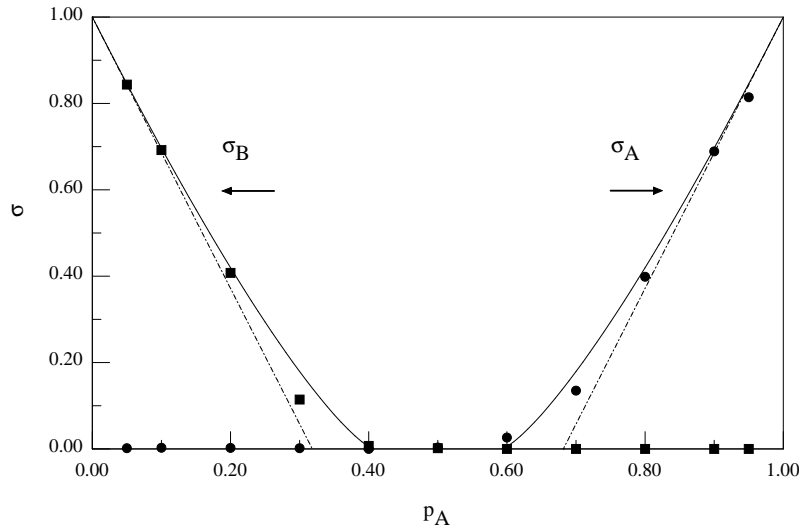


Figure 8. The weights of the delta functions, $\sigma_A(p_A)$ (circles) and $\sigma_B(p_A)$ (squares), as obtained from the reflectance data. The solid curve (—) is from direct simulations of the percolation problem [27]. The dash-dot curve (— · —) is the effective-medium-theory curve. Note that $p_B = 1 - p_A$.

Table 1. The zeroth and first moments, μ_0^A , μ_0^B , and μ_1 of the fitted spectral function. The theoretical values for the moments are given by equations (12) and (15), $\mu_0^A = 1 - p_A$, $\mu_0^B = p_A$, and $\mu_1^{\text{theor}} = p_w p_A (1 - p_A)$.

p_A	μ_0^A	μ_0^B	μ_1	μ_1^{theor}
0.95	0.0559	0.9450	0.0359	0.0324
0.90	0.1039	0.8978	0.0629	0.0614
0.80	0.2076	0.7931	0.1125	0.1091
0.70	0.3064	0.6940	0.1445	0.1432
0.60	0.4057	0.5947	0.1663	0.1636
0.50	0.5015	0.4986	0.1698	0.1704
0.40	0.6013	0.3988	0.1641	0.1636
0.30	0.7011	0.2990	0.1424	0.1432
0.20	0.7953	0.2047	0.1059	0.1091
0.10	0.8998	0.1010	0.0586	0.0614
0.05	0.9463	0.0544	0.0304	0.0324

The zeroth moments μ_0^A and μ_0^B give the area fractions of the two phases and are accurate to better than 0.008. The fitted values for the first moment, μ_1 , are generally accurate to within 4% with somewhat larger percentage errors for $p_A = 0.05$ and $p_A = 0.95$, when the first moment is very small. The accuracies of the zeroth moment and first moment are linked because of equation (18).

The Lagrange multipliers in equation (25) can be adjusted in a fairly systematic way to obtain an optimal fit while suppressing meaningless structure in the spectral function [8, 9]. The first two terms in equation (25) are model independent in the sense that if there is no noise in the data we can fit the reflectance data and satisfy both constraints exactly. The third term is based on the *ad hoc* assumption that the spectral function is reasonably smooth. This constraint

can never be exactly satisfied because a constant spectral function is incompatible with the other constraints. If we impose no constraints on the spectral function, the algorithm quickly converges to a good fit to the reflectance R but results in a meaningless, wildly oscillating spectral function with large positive and negative values. If we only impose the constraint that σ_A , σ_B , and $g(x)$ be non-negative, the algorithm fails to converge in a reasonable number of iterations. For any positive value of λ , the algorithm converges to a spectral function that is almost independent of λ . For all $10^{-4} < \lambda < 1$ there is no noticeable change in the spectral function; for $\lambda < 10^{-6}$ very small changes in g are observed but the principal effect of decreasing λ is that for $\lambda < 10^{-8}$ the rate of convergence deteriorates substantially. We choose to set $\lambda = 1$. The smoothness constraint suppresses meaningless structure in the fitted spectral function. For fixed $\lambda = 1$ we vary λ_{smooth} and monitor χ_R^2 . For $10^{-3} < \lambda_{\text{smooth}} < 10^{-1}$, χ_R^2 is almost constant but increases for larger values of λ_{smooth} . We interpret this to mean that the smoothness constraint suppresses meaningful structure in the spectral function for $\lambda_{\text{smooth}} > 0.1$ but that for $\lambda_{\text{smooth}} < 0.1$ there is structure in the spectral function that cannot be justified by the data. We choose to set $\lambda_{\text{smooth}} = 0.1$.

We illustrate the effect of adjusting λ_{smooth} in figures 9 and 10 where, to make the effect more obvious, we have increased the noise in R by a factor of four. The curves are for $p_A = 0.50$, as in figures 4 and 6. In figure 10 we plot the reduced spectral function, g_0 , as calculated directly in reference [10], and the reduced spectral function, g , extracted from the noisy reflectance data of figure 9 with $\lambda = 1$, $\lambda_{\text{smooth}} = 0.01$ and with $\lambda = 1$, $\lambda_{\text{smooth}} = 1.0$. It is clear that for $\lambda_{\text{smooth}} = 0.01$ there is structure in g that is not present in g_0 . This structure is suppressed in the g obtained with $\lambda_{\text{smooth}} = 1.0$ although the χ_R^2 of the two curves are essentially the same. In this case, because of the increased noise in these reflectance data, the optimal value for λ_{smooth} is 1.0.

Figures 9 and 10 also illustrate the stability of the method for extracting the spectral

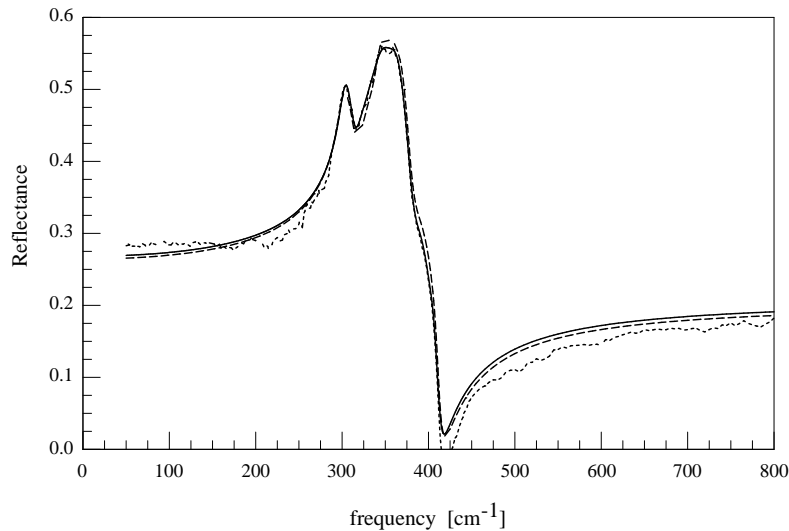


Figure 9. The reflectance, $R(\omega)$, of a 2d square net with random site disorder and the concentration $p_A = 0.50$. The broken curve (---) is the true reflectance, $R_{\text{true}}(\omega)$, as calculated by the simulations. The dashed curve (- - -) is $R_{\text{true}}(\omega)$ with noise added. The solid curve (—) is the fitted $R(\omega)$, which is used to determine the spectral function. The noise has been increased by a factor of 4 compared to that in figure 4.

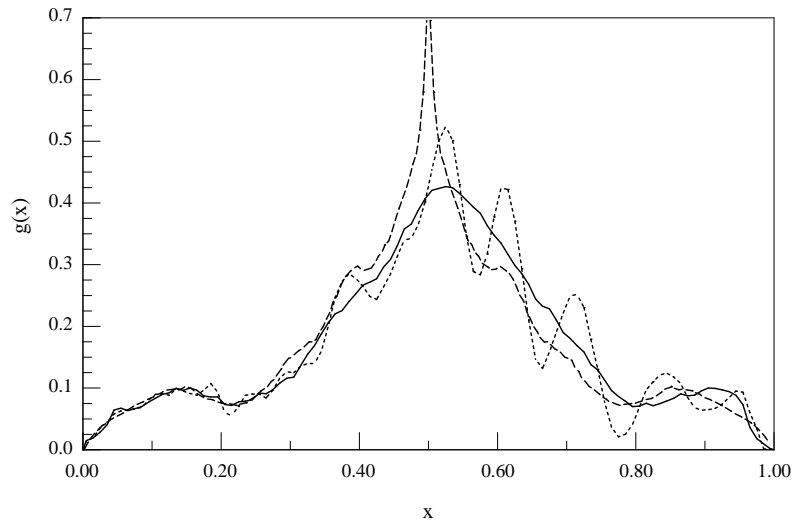


Figure 10. The reduced spectral function $g(x)$ for the 2d square net with random site disorder at $p_A = 0.50$. The broken curve (---) is $g_0(x)$, as calculated in reference [10]. The dashed curve (- - -) is the $g(x)$ obtained from the reflectance data of figure 9 with $\lambda = 1$ and $\lambda_{\text{smooth}} = 0.01$. The solid curve (—) is the $g(x)$ obtained from the reflectance data of figure 9 with $\lambda = 1$ and $\lambda_{\text{smooth}} = 1.0$.

function from the reflectance data. Despite the reflectance data in figure 9 being very noisy, there is a recognizable spectral function in figure 10, which can be compared with figure 6 obtained from data with one quarter the noise. Note that away from the reststrahlen band the fitted reflectance gives a very poor fit to the noisy data because the noisy data are inconsistent with the Hashin–Shtrikman bounds. This emphasizes the importance of having good values for the dielectric functions of the constituent materials, ε_A and ε_B , as input for the fitting algorithm.

5. Conclusions

We have demonstrated that for a two-component model system, with physically reasonable values for the dielectric functions of the two constituent components, it is possible to extract the spectral function from experimentally accessible quantities. Specifically, using numerical simulations of a 2d square net with random site substitution, we calculate the effective reflectance as a function of frequency as we sweep through a dielectric resonance in one of the components. From the reflectance data in the reststrahlen band we are able to extract a spectral function that is in good agreement with that obtained previously by a direct method. Our results are stable against the introduction of noise, both in the simulated reflectance data and the assumed values for the dielectric functions of the pure material.

The results justify an attempt to determine the spectral function for a composite material from actual experimental data. Because the spectral function depends solely on the geometry of the composite and not on the dielectric functions of the components, a test of this approach would be to extract the spectral function independently from two sets of data for the same composite, and compare the resulting spectral functions. For example, if the dielectric function of at least one of the components depends strongly on temperature we could extract the spectral

function independently from reflectance data taken at two different temperatures. Another possibility would be if the pure materials had two or more resonance lines; it should be possible to independently extract the spectral function from the reflectance data spanning each resonance.

Acknowledgments

We acknowledge valuable discussions with A J Sievers on the experimental issues associated with this problem. We thank P F Peterson for his help in the early stages of this project. This work was partially supported by the NSF under grant DMR97-04099

Appendix A. Definition of the reduced spectral function $g(x)$

Using the definition of the normalized dielectric function of the composite, equations (2) and (4), we have

$$\varepsilon = \varepsilon_A \left(1 - \int_0^1 \frac{h_A(x) dx}{s_A - x} \right) = \varepsilon_B \left(1 - \int_0^1 \frac{h_B(x) dx}{s_B - x} \right). \quad (\text{A.1})$$

We simplify the notation by letting $s = s_A = 1 - s_B$, and use $\varepsilon_B/\varepsilon_A = (s - 1)/s$, to obtain

$$1 - \int_0^1 \frac{h_A(x) dx}{s - x} = \frac{s - 1}{s} \left(1 - \int_0^1 \frac{h_B(x) dx}{1 - s - x} \right). \quad (\text{A.2})$$

Collecting terms and rearranging we get

$$\begin{aligned} \int_0^1 \frac{h_A(x) dx}{s - x} &= \frac{1}{s} \left(1 - \int_0^1 \frac{h_B(x) dx}{1 - x} \right) + \left(\int_0^1 \frac{h_B(x) dx}{1 - s - x} - \int_0^1 \frac{h_B(x) dx}{(1 - x)(1 - s - x)} \right) \\ &= \frac{1}{s} m_B(1) - \int_0^1 \frac{x h_B(x) dx}{(1 - x)(1 - s - x)}. \end{aligned} \quad (\text{A.3})$$

Let $s = x_0 + i\epsilon$, where x_0 and ϵ are both real, and take the imaginary part of both the left- and the right-hand side in the limit $\epsilon \rightarrow 0$. From the LHS we get

$$\lim_{\epsilon \rightarrow 0} \text{Im} \left(\int_0^1 \frac{h_A(x) dx}{x_0 + i\epsilon - x} \right) = -\pi h_A(x_0). \quad (\text{A.4})$$

From the RHS we get

$$\begin{aligned} \lim_{\epsilon \rightarrow 0} \text{Im} \left(\frac{1}{x_0 + i\epsilon} m_B(1) - \int_0^1 \frac{x h_B(x) dx}{(1 - x)(1 - x_0 - i\epsilon - x)} \right) \\ = -\pi \delta(x_0) m_B(1) - \pi \frac{1 - x_0}{x_0} h_B(1 - x_0) \end{aligned} \quad (\text{A.5})$$

or

$$h_A(x) = \frac{(1 - x)}{x} h_B(1 - x) + \delta(x) m_B(1). \quad (\text{A.6})$$

Similarly we have

$$h_B(x) = \frac{(1 - x)}{x} h_A(1 - x) + \delta(x) m_A(1). \quad (\text{A.7})$$

Multiplying through by x and noting that $x\delta(x) = 0$, we obtain

$$x h_A(x) = (1 - x) h_B(1 - x) \quad (\text{A.8})$$

from which we define $g(x) = xh_A(x) = (1-x)h_B(1-x)$. We identify $m_B(1) = \sigma_B$ as the dielectric function of the composite if $\varepsilon_A = 0$, and $\varepsilon_B = 1$ or, equivalently, the conductivity of the composite in the percolation problem when the A phase is a void, and the B phase has unit conductivity. From (A.6) we obtain

$$h_A(x) = \frac{g(x)}{x} + \sigma_B \delta(x) \quad (\text{A.9})$$

and similarly from (A.7) we obtain

$$h_B(x) = \frac{g(1-x)}{x} + \sigma_A \delta(x). \quad (\text{A.10})$$

Appendix B. Noise

The noise added to the reflectance data is random Gaussian noise that is smoothed with a window of about 100 cm^{-1} . The smoothing introduces correlations that result in high-frequency random noise superimposed on a low-frequency random background. After the smoothing process the amplitude of the low-frequency component of the noise varied between 0.01 and 0.02 with the amplitude of the high-frequency component about 0.002. This noise can cause appreciable relative errors in the reflectance. For example, in figure 2 the error in $R(\omega)$ around $\omega = 200 \text{ cm}^{-1}$ is about 7%. In figure 4 the error in $R(\omega)$ around $\omega = 410 \text{ cm}^{-1}$ is over 100%. For some values of p we checked the fitting procedure with the noise in R increased by factors of two and four. χ_R^2 increases, as expected, and the quality of the spectral function obtained deteriorates in a systematic way.

References

- [1] Maxwell J C 1873 *Electricity and Magnetism* 1st edn (Oxford: Clarendon)
- [2] Beran M 1968 *Statistical Continuum Theories* (New York: Interscience)
- [3] Hashin Z 1983 *J. Appl. Mech.* **50** 481–505
- [4] Bergman D J 1978 *Phys. Rep.* **43** 378–407
Bergman D J 1979 *J. Phys. C: Solid State Phys.* **12** 4947–60
Bergman D J 1980 *Phys. Rev. Lett.* **44** 1285–7
Bergman D J 1981 *Phys. Rev. B* **23** 3058–65
Bergman D J 1982 *Ann. Phys., NY* **138** 78–114
- [5] Milton G W 1980 *Appl. Phys. Lett.* **37** 300–2
Milton G W 1981 *Phys. Rev. Lett.* **46** 542–5
Milton G W 1981 *J. Appl. Phys.* **52** 5286–93
Milton G W 1981 *J. Appl. Phys.* **52** 5294–304
- [6] Stroud D, Milton G W and De B R 1986 *Phys. Rev. B* **34** 5145–53
- [7] Ghosh K and Fuchs R 1988 *Phys. Rev. B* **38** 5222–36
- [8] Press W H, Teukolsky S A, Vetterling W T and Flannery B P 1996 *Numerical Recipes in FORTRAN: The Art of Scientific Computing* 2nd edn (Cambridge: Cambridge University Press) pp 779–817
- [9] Cowan G 1998 *Statistical Data Analysis* (Oxford: Clarendon) pp 153–87
- [10] Day A R and Thorpe M F 1996 *J. Phys.: Condens. Matter* **8** 4389–409
- [11] Golden K and Papanicolaou G 1983 *Commun. Math. Phys.* **90** 473–94
- [12] Korrington J 1984 *Geophysics* **49** 1760–2
- [13] Stauffer D 1985 *Introduction to Percolation Theory* 1st edn (London: Taylor and Francis)
- [14] Jonckheere T and Luck J M 1998 *J. Phys. A: Math. Gen.* **31** 3687–717
- [15] Bruno O and Golden K 1990 *J. Stat. Phys.* **61** 365–86
- [16] Landau L D and Lifshitz E M 1960 *Electrodynamics of Continuous Media* (London: Pergamon) pp 45–7
- [17] Miller M N 1969 *J. Math. Phys.* **10** 1988–2004
- [18] Thorpe M F and Tang W 1987 *J. Phys.: Condens. Matter* **20** 3925–38
- [19] Mitra S S 1985 *Handbook of Optical Constants of Solids* ed E D Palik (Orlando, FL: Academic) pp 213–70
- [20] Hinsen K and Felderhof B U 1992 *Phys. Rev. B* **46** 12 955–63

- [21] Wooten F 1972 *Optical Properties of Solids* (New York: Academic)
- [22] Milton G W 1998 Private communication
- [23] See Press W H, Teukolsky S A, Vetterling W T and Flannery B P 1996 *Numerical Recipes in FORTRAN: The Art of Scientific Computing* 2nd edn (Cambridge: Cambridge University Press) pp 678–83
- [24] Aspnes D E 1985 *Handbook of Optical Constants of Solids* ed E D Palik (Orlando, FL: Academic) pp 89–112
- [25] Hashin Z and Shtrikman S 1962 *J. Appl. Phys.* **33** 3125–31
- [26] Frank D J and Lobb C J 1988 *Phys. Rev. B* **37** 302–7
- [27] Watson B P and Leath P L 1974 *Phys. Rev. B* **9** 4893–6